Chapter 4

Phase Segregation in Mixed Nb-Sb Double Perovskites $Ba_2LnNb_{1-x}Sb_xO_6$

4.1 Introduction

The properties of perovskites are known to be strongly influenced by the precise structure of these oxides, as exemplified by the recent illustration of switching from ferromagnetism to antiferromagnetism in A_2CrSbO_6 by Retuerto *et al.*[1]. In particular some properties such as colossal magneto-resistance and ferroelectricity tend to be most prominent in compounds close to a structural instability that may take the form of a phase transition or a solubility limit[2]. This is extremely well documented for ferroelectrics based on Pb-Zr-Ti (PZT) perovskites where optimal performance occurs near the morphotropic phase boundary[3, 4].

The chemistry and structures of perovskites containing Nb^{5+} and Sb^{5+} provides a number of examples of unexpected structural complexity and instability. The similar charge and ionic radii of Sb^{5+} (0.60 Å[5]) and Nb^{5+} (0.64 Å[5]) leads to the assumption that antimonate and niobate compounds should adopt similar perovskite structures. There are, however, numerous examples in the perovskite family where the niobate and antimonate compounds adopt different structures or where the antimonate but not the corresponding niobate, or vice versa, forms. Examples where the antimonate but not the corresponding niobate exists include Ba_2BiSbO_6[6] and $Ba_4NaSb_3O_{12}$[7] while the Aurivillius phase $BaBi_2Nb_2O_9$[8] is known to exist but $BaBi_2Sb_2O_9$ is unknown. The results presented in Chapter 3, on the other hand, indicate that while the two series Ba_2LnNbO_6 and Ba_2LnSbO_6 (Ln = lanthanide or Y^{3+}) both form they adopt subtly different structures. It was found that while the majority of the niobates adopt an *I*4/*m* tetragonal ($a^0a^0c^-$) symmetry between *I*2/*m* monoclinic ($a^-a^-c^0$) and $Fm\bar{3}m$ cubic ($a^0a^0a^0$) structures the antimonates adopt the $R\bar{3}$ intermediate ($a^-a^-a^-$) instead. These observations led to the conclusion that both the presence of π-bonding and the ionic radius of the lanthanide have a strong influence on which intermediate is adopted. This seems to suggest that the intermediate phase adopted by the $Ba_2LnB'O_6$

family of compounds lies on a cusp of an instability between two alternate structures and seemingly small differences in the composition of specific compounds in these series play an important role in the formation and stability of one structure compared to the other.

Further understanding of the chemical basis for the differences between Nb^{5+} and Sb^{5+} containing perovskites is clearly needed. Although superficially similar and having practically identical tolerance factors (0.970 for both compounds[5, 9, 10]) the two oxides Ba_2PrSbO_6 and Ba_2EuNbO_6 adopt alternate intermediate structures, $R\bar{3}$ and *I*4/*m* respectively, at room temperature. Structural studies of solid solutions of the type $Ba_2Eu_{1-x}Pr_xNb_{1-x}Sb_xO_6$ are, therefore, expected to shed light on the chemical differences between Nb^{5+} and Sb^{5+}, while also providing further insight into the complex phase transition behaviour in $Ba_2LnB'O_6$ oxides. A related study by Mitchell and co-workers[11] on the series $Sr_{1-2x}Na_xLa_xTiO_3$ (solid solution between $SrTiO_3$ and $Na_{0.5}La_{0.5}TiO_3$) concluded that the transition from *I*4/*mcm* to $R\bar{3}c$ occurs directly via a discontinuous phase transition[12]. The *I*4/*mcm* to $R\bar{3}c$ transition in these ABO_3 perovskites involves the same two Glazer tilt systems, $a^0a^0c^-$ and $a^-a^-a^-$, as an *I*4/*m* to $R\bar{3}$ transition that may occur in the $A_2BB'O_6$ double perovskite series $Ba_2Eu_{1-x}Pr_xNb_{1-x}Sb_xO_6$. The difference in symmetry between the two series is a consequence of the ordering of the two different B-site cations in the case of $Ba_2Eu_{1-x}Pr_xNb_{1-x}Sb_xO_6$.

The tetragonal to rhombohedral phase transition in $Ba_2Eu_{1-x}Pr_xNb_{1-x}Sb_xO_6$ may be first order, as seen for $Sr_{1-2x}Na_xLa_xTiO_3$, or it may involve an intermediate phase. This would most likely be either *I*2/*m* monoclinic ($a^-a^-c^0$) or $Fm\bar{3}m$ cubic ($a^0a^0a^0$) both of which are observed in the two $Ba_2LnB'O_6$, B' = Nb^{5+} or Sb^{5+}, series. Alternatively, the different structures observed for Ba_2PrSbO_6 and Ba_2EuNbO_6 may indicate that Nb^{5+} and Sb^{5+} are incompatible in the same perovskite structure. Such incompatibility could manifest itself as a miscibility gap that would lead to segregation and the formation of two or more phases with different chemical compositions. The occurrence of any segregation would be consistent with the apparent chemical incompatibility of niobium and antimony perovskites mentioned previously.

In order to determine which of these three possibilities (direct first order phase transition, presence of an intermediate phase or phase segregation) occurs two series of oxides, $Ba_2Eu_{1-x}Pr_xNb_{1-x}Sb_xO_6$ and $Ba_2NdNb_{1-x}Sb_xO_6$ have been synthesised and then structurally characterised using synchrotron X-ray diffraction and, as required, analytical electron microscopy. These oxides were chosen to minimise the changes in volume and tolerance factor across the series. That is, the only significant difference across each series will be the exchange of Sb^{5+} for Nb^{5+}. The high resolution of synchrotron X-ray diffraction is particularly important to this study in regards to determining whether these samples consist of single or multiple perovskite phases.

4.2 Synthesis of $Ba_2LnNb_{1-x}Sb_xO_6$

Samples of $Ba_2Eu_{1-x}Pr_xNb_{1-x}Sb_xO_6$ and $Ba_2NdNb_{1-x}Sb_xO_6$ (x = 0, 0.1, 0.2,…, 1) were prepared from stoichiometric mixtures of $BaCO_3$, Nb_2O_5, Sb_2O_3 and the appropriate lanthanide oxides; Pr_6O_{11}, Nd_2O_3 and Eu_2O_3. The appropriate starting mixtures were finely ground as an acetone slurry in an agate mortar and pestle. After drying samples were heated, in alumina crucibles, for a period of 24 hrs at 800 °C followed by heating at 1000 °C, 1100 °C and 1200 °C for periods of 24 hrs. The samples were then pressed into pellets and heated at 1300 °C for 24 hrs followed by heating, in pelleted form, for a maximum of 48 hrs at 1350 °C and 24 hrs at 1400 °C in order to yield samples with the maximum purity. In all cases samples were reground and, if required, repelleted after each heating period. Laboratory X-ray diffraction was used throughout this process to determine the best procedure for obtaining highly crystalline, pure, powder samples.

4.3 Experimental Method

Synchrotron X-ray diffraction patterns were recorded, at ambient temperature, for all samples on the Debye-Scherrer diffractometer at the ANBF, beamline 20B at the Photon Factory, Tsukuba, Japan. Variable temperature measurements, at temperatures of up to 500 °C were also carried out on $Ba_2Eu_{0.8}Pr_{0.2}Nb_{0.8}Sb_{0.2}O_6$ and $Ba_2NdNb_{0.5}Sb_{0.5}O_6$. These measurements were recorded using a wavelength of 0.80073(1) or 0.80286(1) Å and were carried out as described in Section 2.2.2.1.

4.4 Results and Discussion

In this section results regarding the structures of the series $Ba_2Eu_{1-x}Pr_xNb_{1-x}Sb_xO_6$ and $Ba_2NdNb_{1-x}Sb_xO_6$ will be initially presented followed by an explanation of the behaviour of these two series.

4.4.1 Structures of $Ba_2Eu_{1-x}Pr_xNb_{1-x}Sb_xO_6$

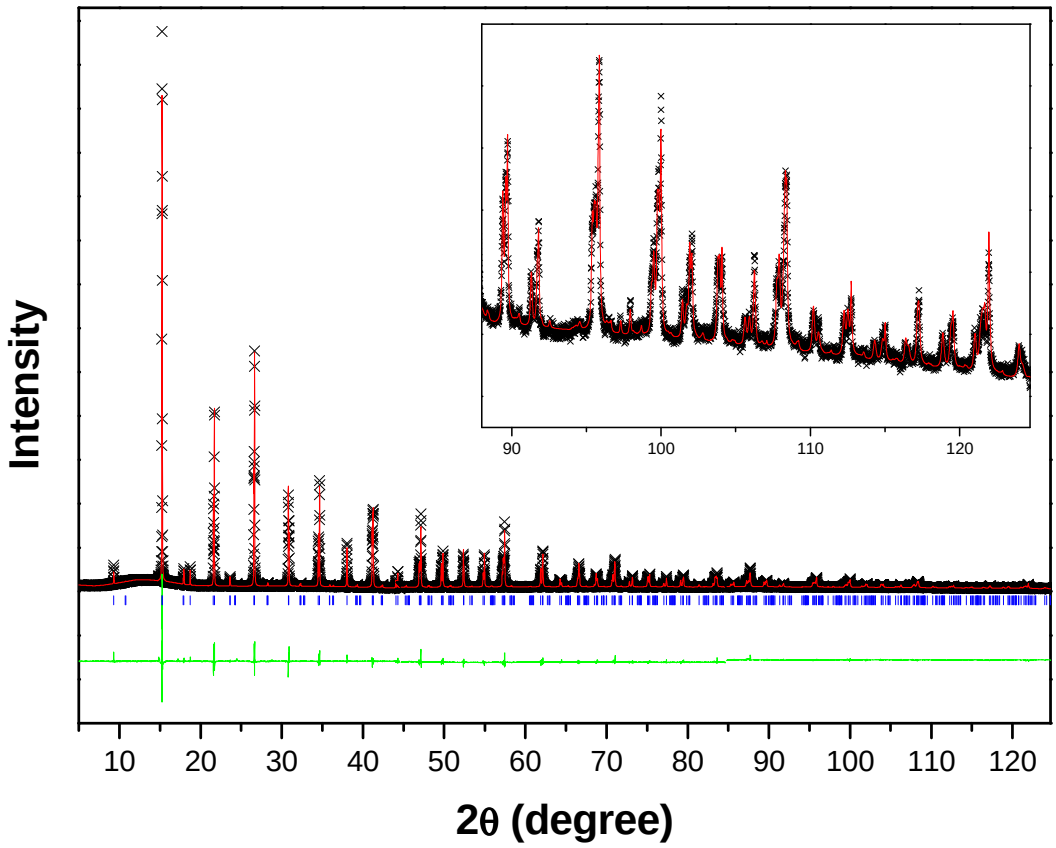

Figure 4.1: Synchrotron X-ray diffraction pattern of Ba_2EuNbO_6. The insert shows both the high quality of data obtained out to high 2θ and the splitting indicative of tetragonal symmetry. The crosses, upper and lower continuous lines represent the observed and calculated intensities and the difference between these respectively. The vertical markers show the positions of the allowed Bragg reflections.

As expected from Chapter 3 the synchrotron X-ray diffraction patterns of the end member compounds in the series $Ba_2Eu_{1-x}Pr_xNb_{1-x}Sb_xO_6$ had peak splitting and super-lattice reflection conditions consistent with a $R\bar{3}$ rhombohedral structure for Ba_2PrSbO_6, x = 1, and $I4/m$ tetragonal symmetry for Ba_2EuNbO_6, x = 0 (see Figures

4.1 and 4.2). Subsequent refinements of models in the appropriate symmetry gave good fits to the patterns (see Table 4.1 and Figure 4.3 for unit cell parameters). The compounds with $0.5 \leq x \leq 0.9$ were also found to be rhombohedral exhibiting the same peak splitting pattern as Ba_2PrSbO_6. There was no evidence in the refinements for any of the samples having significant disorder of the lanthanide and B' cations.

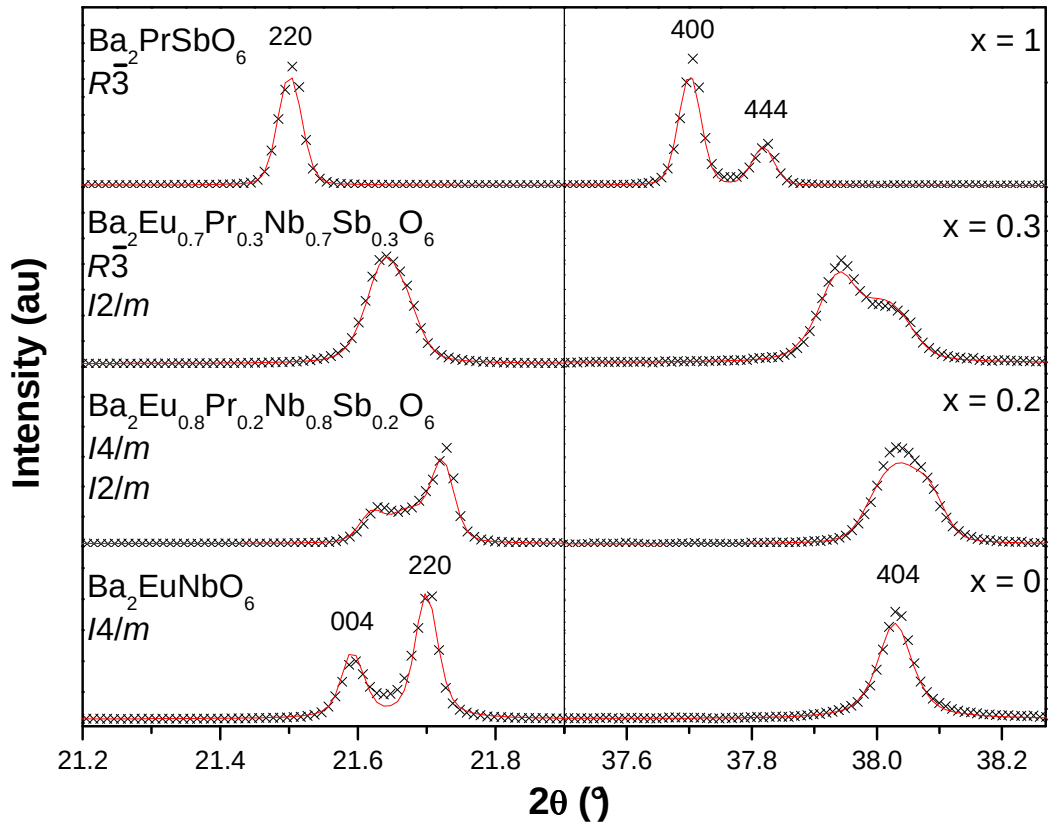

Figure 4.2: Selected regions of patterns belonging to compounds in the series $Ba_2Eu_{1-x}Pr_xNb_{1-x}Sb_xO_6$ indicating the various symmetries adopted by these materials. The crosses and continuous line represent the observed and calculated intensities respectively. The diffraction patterns have been rescaled to better illustrate the changes, with the parent (444) reflection near $2\theta = 38.0°$ being ~ $1/5^{th}$ as intense as the cubic (400) reflection near $2\theta = 21.6°$. The indices given in the figure are those for the listed space group.

Table 4.1: Phase composition and unit cell parameters for the $Ba_2Eu_{1-x}Pr_xNb_{1-x}Sb_xO_6$ series of compounds determined using synchrotron X-ray diffraction. In the case of the *I*2/*m* phases in the x = 0.3 and 0.4 samples the monoclinic angle was unstable in the refinement and therefore was set to 90°.

x	Space Group	*a* (Å)	*b* (Å)	*c* (Å)	α (°)	β (°)	Volume (Å^3)	Phase Composition (mol %)
0	*I*4/*m*	6.00428(4)	= *a*	8.53304(7)	90	90	307.627(4)	100
0.1	*I*4/*m*	6.00912(2)	= *a*	8.53734(6)	90	90	308.279(3)	56(1)
	*I*2/*m*	6.03259(7)	6.01278(6)	8.49726(6)	90	90.046(1)	308.217(5)	44(1)
0.2	*I*4/*m*	6.01522(21)	= *a*	8.54172(52)	90	90	309.106(22)	27(1)
	*I*2/*m*	6.03787(5)	6.01891(5)	8.50632(7)	90	90.034(1)	309.132(4)	73(3)
0.3	$R\bar{3}$	6.02243(6)	= *a*	= *a*	60.1212(18)	= α	154.922(118)	31(1)
	*I*2/*m*	6.04072(8)	6.02267(7)	8.51378(9)	90	90	309.727(8)	69(2)
0.4	$R\bar{3}$	6.02493(5)	= *a*	= *a*	60.1331(10)	= α	155.113(64)	62(2)
	*I*2/*m*	6.04355(18)	6.02582(14)	8.51677(25)	90	90	310.158(15)	38(1)
0.5	$R\bar{3}$	6.02871(3)	= *a*	= *a*	60.124(5)	= α	155.373(35)	100
0.6	$R\bar{3}$	6.03344(4)	= *a*	= *a*	60.118(7)	= α	155.716(46)	100
0.7	$R\bar{3}$	6.03719(2)	= *a*	= *a*	60.1353(4)	= α	156.069(26)	100
0.8	$R\bar{3}$	6.04188(2)	= *a*	= *a*	60.1335(4)	= α	156.423(29)	100
0.9	$R\bar{3}$	6.04784(4)	= *a*	= *a*	60.1485(5)	= α	156.935(35)	100
1.0	$R\bar{3}$	6.05272(1)	= *a*	= *a*	60.1483(2)	= α	157.323(15)	100

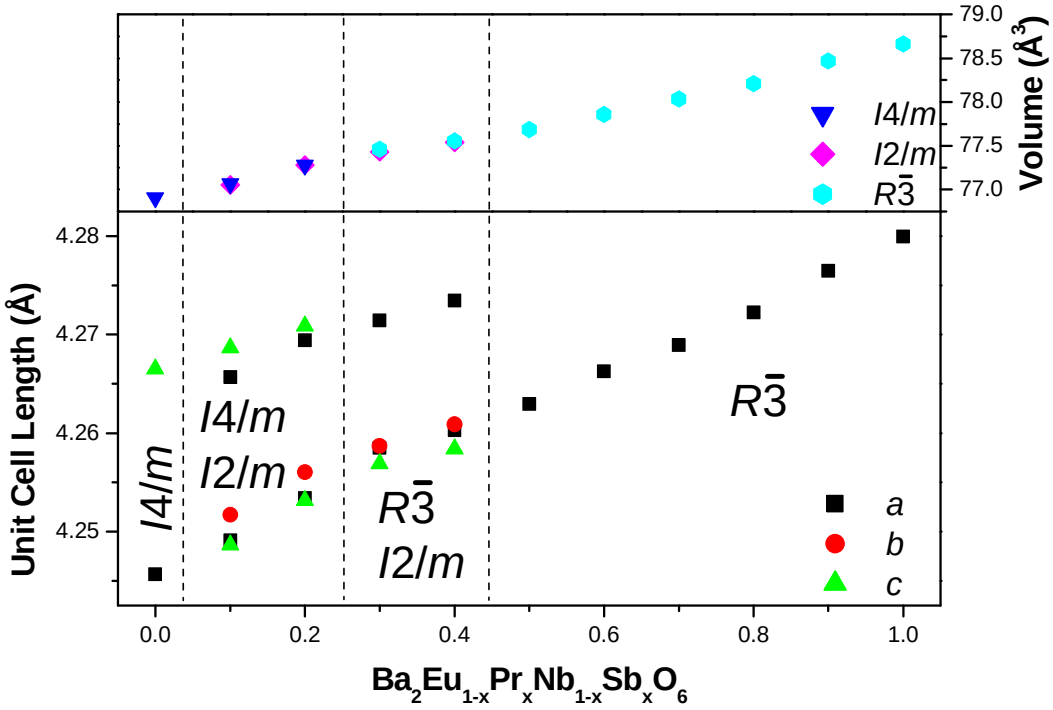

Figure 4.3: Variation of the unit cell lengths and volumes for compounds in the series $Ba_2Eu_{1-x}Pr_xNb_{1-x}Sb_xO_6$. The parameters have been reduced to the size of the primitive perovskite structure. Note the systematic variation in volume across the series and the near-identical volumes of the co-existing phases in both two phase regions.

The diffraction patterns of the compounds with $0.1 \leq x \leq 0.4$ were not well fitted by either single or two-phase models in $R\bar{3}$ and/or *I*4/*m*. The diffraction patterns of these compounds contained only *R*-point super-lattice reflections with no evidence for any *M*- or *X*-point reflections being found. This indicates that the structure has only out-of-phase tilts and/or cation ordering, the later having been shown to exist in all members of the $Ba_2LnB'O_6$ family. Discarding the tetragonal and rhombohedral structures shown not to fit the observed diffraction data, the group theoretical analysis by Howard *et al.*[12] indicates there are only three other possibilities that have either no tilts or only out-of-phase tilts. These are $P\bar{1}$ triclinic (tilt system $a^-b^-c^-$), *I*2/*m* monoclinic ($a^-a^-c^0$) and $Fm\bar{3}m$ cubic ($a^0a^0a^0$). The diffraction patterns of the compounds with $0.1 \leq x \leq 0.4$ were all inconsistent with single phase models for any of these structures.

Since other members in the $Ba_2LnB'O_6$ series are known to have structures in *I*2/*m* and $Fm\bar{3}m$ the possibility that the samples of $Ba_2Eu_{1-x}Pr_xNb_{1-x}Sb_xO_6$ with $0.1 \leq x \leq 0.4$ are a mixture of two phases, *I*4/*m* or $R\bar{3}$ with *I*2/*m* or $Fm\bar{3}m$, was considered. Extensive testing of all the various possibilities suggested that, for the two oxides with x = 0.1 and 0.2, the combination of *I*4/*m* and *I*2/*m* was appropriate. The final R-factors for the *I*2/*m* and *I*4/*m* model for the x = 0.2 sample, R_p = 4.8 and R_{wp} = 6.2 %, were noticeably better than those for the next best model of $R\bar{3}$ and *I*4/*m*, R_p = 7.8 and R_{wp} 10.3 %. For the two samples with x = 0.3 and 0.4 the best fits were obtained with a mixture of $R\bar{3}$ and *I*2/*m*. For the x = 0.3 sample R_p = 3.6 and R_{wp} = 4.7 % in this model compared to values of 6.4 and 6.0 % in the $R\bar{3}$ / *I*4/*m* model. The change in phase compositions results in the striking difference between the diffraction patterns of the x = 0.2 and 0.3 samples illustrated in Figure 4.2. For the x = 0.2 sample the splitting of the cubic (400) reflection near 2θ = 21.7° is more pronounced that that of the (444) reflection near 2θ = 38.0°, while in the x = 0.3 sample the splitting of the (444) reflection is clearly greater than that of the (400) reflection.

The presence of the *I*2/*m* structure in the two phase region of $Ba_2Eu_{1-x}Pr_xNb_{1-x}Sb_xO_6$ suggests that the structure changes from *I*4/*m* tetragonal to *I*2/*m* monoclinic to $R\bar{3}$ rhombohedral with increasing x (see Figure 4.3). The sequence of phase transitions seen here is different from that found by Mitchell *et al.* for $Sr_{1-2x}Na_xLa_xTiO_3$[11] where the transition from tetragonal ($a^0a^0c^-$) to rhombohedral ($a^-a^-a^-$) structure occurred directly, with no indication of an intermediate symmetry being adopted. The atomic positions and bonding environments of the single phase compounds in the series $Ba_2Eu_{1-x}Pr_xNb_{1-x}Sb_xO_6$ are very similar to those presented for the $Ba_2LnB'O_6$ compounds in Chapter 3 and it was not possible to determine precise and accurate values of these parameters in the two phase samples because they were only examined using X-ray diffraction. Therefore for the sake of brevity the reader is referred to the tables presented in that chapter and the results presented in the Appendices.

The two phase transitions, *I*4/*m* to *I*2/*m* and *I*2/*m* to $R\bar{3}$, must both be discontinuous according to Landau theory[12], and this may account for the co-existence of the two phases. It is also possible that the co-existence of the two phases reflects a solubility limit of the Nb^{5+} and Sb^{5+} cations across the series leading to segregation into two

phases with different chemical compositions. To investigate this, variable temperature synchrotron X-ray diffraction patterns of $Ba_2Eu_{0.8}Pr_{0.2}Nb_{0.8}Sb_{0.2}O_6$ were collected up to a maximum temperature of 500 °C. If the presence of the two phases, evident at room temperature, is caused by an incomplete first-order phase transition it would be expected that the transition to the higher symmetry structure would be completed at some temperature in this range. The diffraction patterns of $Ba_2Eu_{0.8}Pr_{0.2}Nb_{0.8}Sb_{0.2}O_6$ demonstrated the co-existence of two perovskite-type phases up to 500 °C, with the pattern at 500 °C being most consistent with the presence of two cubic structures. The persistence of the two phases over a temperature range of 500° is a clear indication that the two phase region in this series is caused by inhomogenties due to a solubility limit of one or more of the cations in the solution. Despite this phase segregation the volume change across the series $Ba_2Eu_{1-x}Pr_xNb_{1-x}Sb_xO_6$ does not show any significant discontinuities (see Figure 4.3). This Vegard-like volume expansion indicates that the segregation in the two phase region must be relatively small in contrast to the large discontinuities which would be expected if phase segregation was more significant. It should also be noted that the models refined for the two phase samples were insensitive to any preferential segregation of the B-site cations and final refinements were therefore carried out such that both phases had the same stoichiometry despite the strong evidence for the presence of such segregation.

4.4.2 Structures of $Ba_2NdNb_{1-x}Sb_xO_6$

The second series of mixed Nb-Sb perovskites studied was $Ba_2NdNb_{1-x}Sb_xO_6$. The diffraction pattern of Ba_2NdNbO_6 was well fitted in an *I*2/*m* model while the pattern of Ba_2NdSbO_6 showed the structure to be $R\bar{3}$ rhombohedral (see Figure 4.4). These results are consistent with those presented in Chapter 3. The patterns for the antimony rich compounds (x = 0.8 and 0.9) in the series $Ba_2NdNb_{1-x}Sb_xO_6$ were well fitted by the rhombohedral model. The diffraction patterns of the other intermediate compounds ($0.1 \leq x \leq 0.7$), however, were not consistent with a single phase structure, in either monoclinic or rhombohedral symmetry. In all cases the fit using a single phase model was poor. A significantly better fit was obtained for these compounds using a two phase model of monoclinic and rhombohedral symmetry (see Figure 4.4).

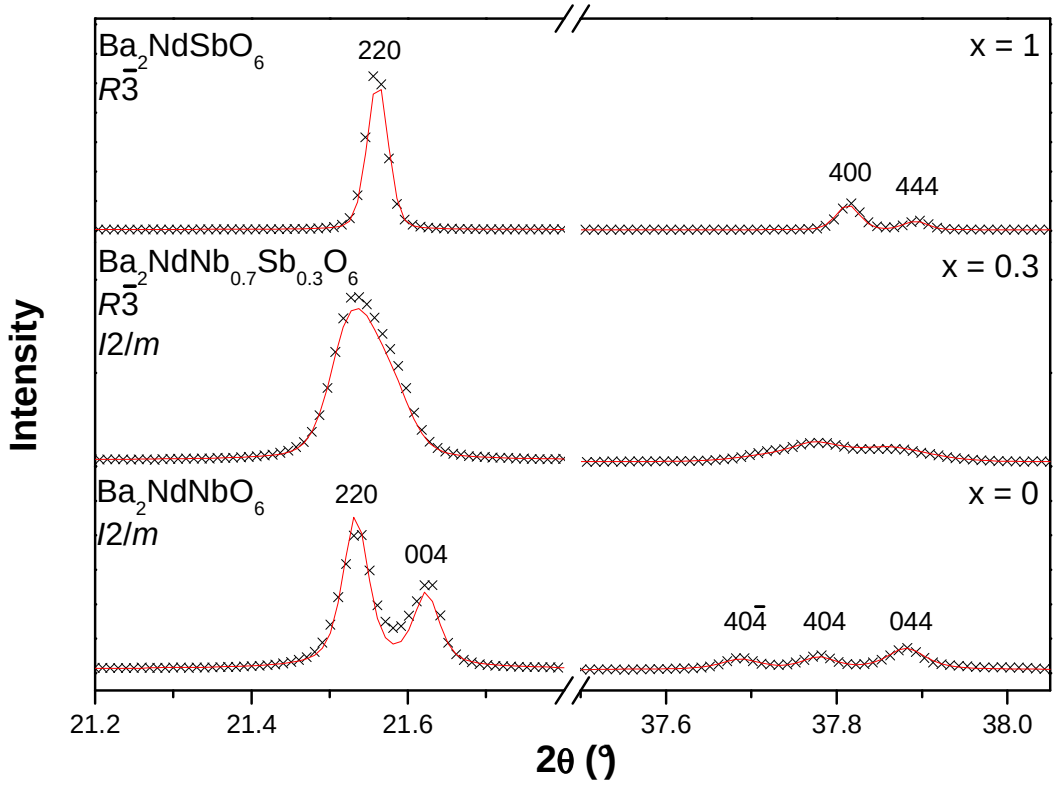

Figure 4.4: Selected regions of diffraction patterns of compounds in the series $Ba_2NdNb_{1-x}Sb_xO_6$ illustrating the various symmetries adopted. The format is the same as in Figure 4.2

It should be noted that the higher resolution available using synchrotron X-ray diffraction was essential in establishing the co-existence of the $R\bar{3}$ and $I2/m$ phases in this series, diffraction patterns obtained using conventional (laboratory) X-ray diffraction were well fitted by single phase models using either rhombohedral or monoclinic symmetry. The failure to detect the two phases using laboratory based diffraction is believed to be a consequence of the similarity of the volume of the two end member oxides Ba_2NdNbO_6 and Ba_2NdSbO_6 (78.510(1) $Å^3$ and 78.108(7) $Å^3$ respectively when reduced to the size of the primitive cubic perovskite unit cell). Clearly considerable care is required in order to confirm if single phase compounds have been formed in such cases and suggests that there may be cases in the literature where compounds are purported to be single phase based on conventional X-ray diffraction when they are in fact a mixture of different perovskite phases. Unit cell parameters for the compounds are listed in Table 4.2 and displayed in Figure 4.5. It was not possible to determine accurate crystallographic details for the two phase samples so the reader is referred to those provided for the end members in Chapter 3.

Table 4.2: Phase composition and unit cell parameters for the $Ba_2NdNb_{1-x}Sb_xO_6$ series of compounds determined using synchrotron X-ray diffraction. In the case of the *I*2/*m* phases in the x = 0.6 and 0.7 samples the monoclinic angle was unstable in the refinement and was therefore set to 90°.

x	Space Group	*a* (Å)	*b* (Å)	*c* (Å)	α (°)	β (°)	Volume (Å^3)	Phase Composition (mol %)
0	*I*2/*m*	6.08122(5)	6.04670(5)	8.54025(7)	90	90.1430(4)	314.038(5)	100
0.1	*I*2/*m*	6.07846(5)	6.04537(5)	8.53931(7)	90	90.1314(4)	313.788(4)	93.8(6)
	$R\bar{3}$	6.04119(16)	= *a*	= *a*	60.3530(51)	= α	156.374(335)	6.3(2)
0.2	*I*2/*m*	6.07160(6)	6.04261(6)	8.53729(9)	90	90.1052(6)	313.211(6)	84.3(6)
	$R\bar{3}$	6.03955(18)	= *a*	= *a*	60.1590(34)	= α	156.338(225)	15.6(4)
0.3	*I*2/*m*	6.06870(8)	6.04189(9)	8.53906(14)	90	90.0802(13)	313.103(8)	64.7(7)
	$R\bar{3}$	6.04103(19)	= *a*	= *a*	60.1394(30)	= α	156.379(198)	35.3(6)
0.4	*I*2/*m*	6.06920(7)	6.04189(14)	8.54022(12)	90	90.0828(12)	313.151(9)	69.0(6)
	$R\bar{3}$	6.04371(22)	= *a*	= *a*	60.0695(60)	= α	156.397(376)	31.0(5)
0.5	*I*2/*m*	6.07185(9)	6.04437(13)	8.54369(18)	90	90.0758(23)	313.586(11)	60.5(1.6)
	$R\bar{3}$	6.04403(14)	= *a*	= *a*	60.0731(36)	= α	156.414(291)	39.5(1.1)
0.6	*I*2/*m*	6.06611(15)	6.04057(28)	8.54064(36)	90	90	312.952(23)	31.6(1.4)
	$R\bar{3}$	6.04182(18)	= *a*	= *a*	60.0876(25)	= α	156.262(184)	68.4(3.0)
0.7	*I*2/*m*	6.06250(17)	6.03939(19)	8.54396(35)	90	90	318.834(19)	31.8(1.5)
	$R\bar{3}$	6.04169(6)	= *a*	= *a*	60.1084(8)	= α	156.322(55)	68.2(3.0)
0.8	$R\bar{3}$	6.04187(5)	= *a*	= *a*	60.0799(9)	= α	156.287(57)	100
0.9	$R\bar{3}$	6.03912(3)	= *a*	= *a*	60.0883(4)	= α	156.035(25)	100
1.0	$R\bar{3}$	6.04069(1)	= *a*	= *a*	60.0998(2)	= α	156.216(13)	100

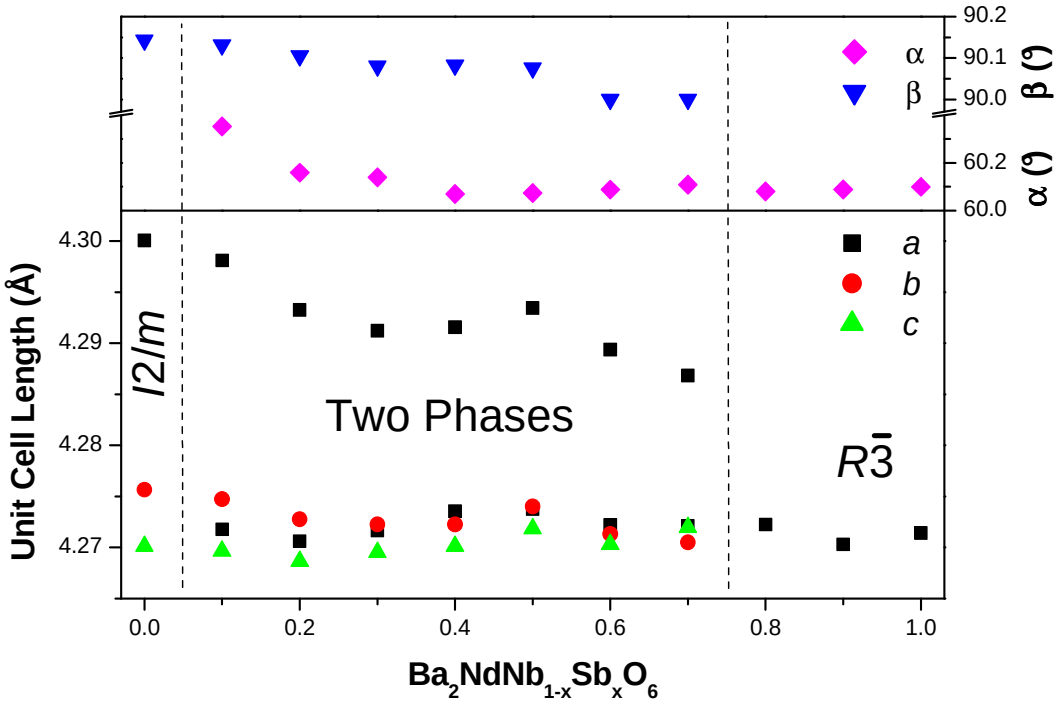

Figure 4.5: Reduced lattice parameters for $Ba_2NdNb_{1-x}Sb_xO_6$ indicating the large two phase region formed in this series.

The existence of this large two phase region in the $Ba_2NdNb_{1-x}Sb_xO_6$ series (see Figure 4.5) is surprising given the relative ease of preparation of the two end member oxides. Phase transitions between structures in *I*2/*m* and $R\bar{3}$ have been observed in numerous double perovskites including Ba_2LnSbO_6 (see Chapter 3) and Ba_2LnBiO_6[13] and are often characterised by a two phase region. An *I*2/*m* to $R\bar{3}$ phase transition is required by Landau theory to be first order[12] and the co-existence of both phases is often characteristic of a first order transition. That the two phase region persists over such a wide range of compositions, however, strongly suggests that significant segregation between the two phases occurs. Diffraction patterns obtained for $Ba_2NdNb_{0.5}Sb_{0.5}O_6$ at temperatures of up to 500 °C demonstrated that the sample was two phase over this temperature range, with two cubic phases being found to co-exist at the maximum temperature examined (see Figure 4.6). This observation is analogous to that seen in $Ba_2Eu_{0.8}Pr_{0.2}Nb_{0.8}Sb_{0.2}O_6$ and indicates that the two phase region in both series is a result of insolubility of the cations, albeit at different points in the phase diagram. It should be noted that, similarly to $Ba_2Eu_{1-x}Pr_xNb_{1-x}Sb_xO_6$, the models refined for two phase samples in the $Ba_2NdNb_{1-x}Sb_xO_6$ series were insensitive

to the presence of any B-site cation segregation so final refinements were carried out so that both phases had the same stoichiometry despite the evidence for segregation.

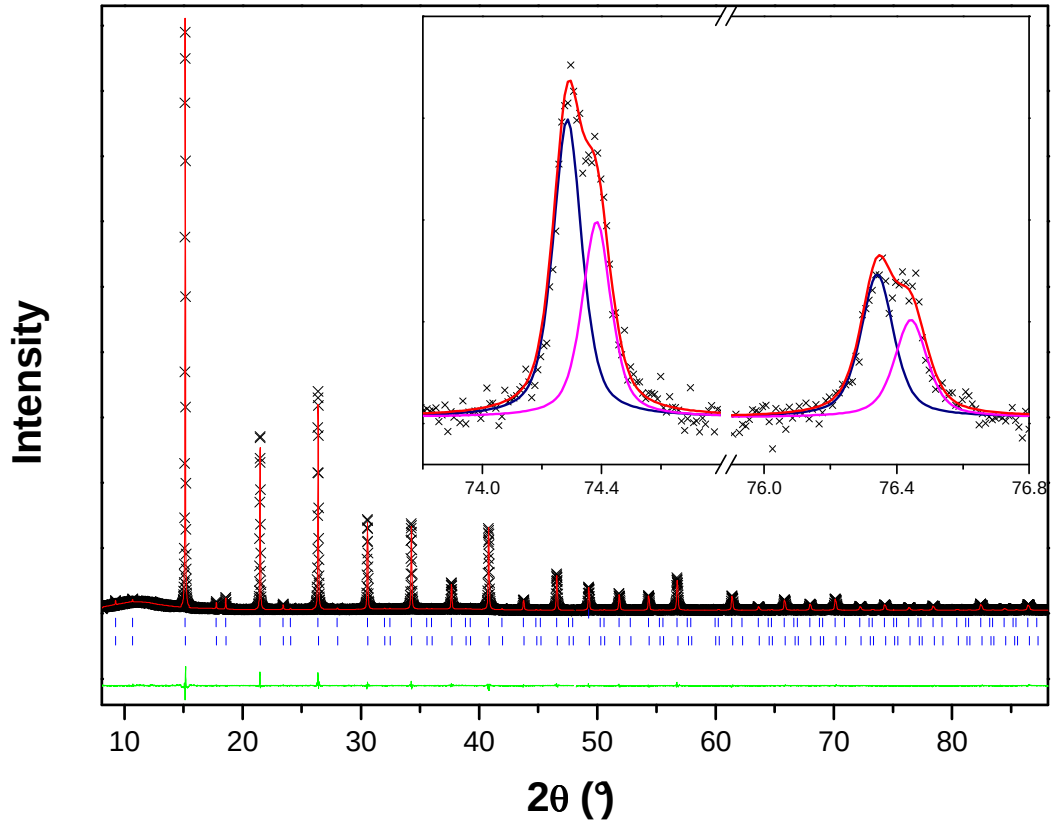

Figure 4.6: Synchrotron X-ray diffraction pattern of $Ba_2NdNb_{0.5}Sb_{0.5}O_6$ at 500 °C. The format is the same as for Figure 4.1. The insert indicates the calculated intensities of the two cubic phases in the sample and the overall calculated intensity.

4.4.3 Phase Segregation

The synchrotron X-ray diffraction patterns of both the series $Ba_2NdNb_{1-x}Sb_xO_6$ and $Ba_2Eu_{1-x}Pr_xNb_{1-x}Sb_xO_6$ demonstrated that a limit in the solubility occurs. Consequently the chemical composition of selected samples (x = 0.2, 0.4, 0.6 and 0.8) was investigated using a combination of Scanning Electron Microscopy (SEM) and Energy Dispersive X-ray (EDX) analysis. Backscattered SEM images did not reveal any strongly contrasting regions suggesting the samples were relatively homogeneous on the scale investigated (see Figure 4.7). The EDX measurements did not identify any regions that contained only Nb^{5+} or Sb^{5+}, although the estimated standard deviations of the Nb^{5+} content, while not large, was noticeably higher in the two phase

regions compared to the samples known to be single phase. Higher spatial resolution is required to establish the precise composition of the individual phases present. Nevertheless it is clear from the microscopy and diffraction measurements that a distinct miscibility gap occurs in these systems. It is, of course, possible that alternate preparation methods could limit the size of this gap.

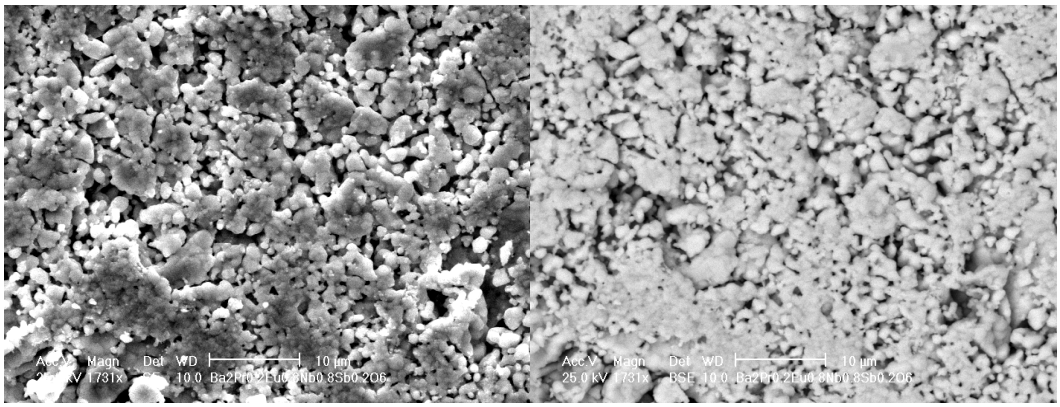

Figure 4.7: Secondary (left) and backscattered (right) electron images of $Ba_2Eu_{0.8}Pr_{0.2}Nb_{0.8}Sb_{0.2}O_6$. The lack of contrast in the backscattered image suggests the sample is relatively homogeneous.

That an inhomogeneity in the distribution of Nb^{5+} appears to be related to the two phase region in both series suggests that it may not be possible to simultaneously accommodate Nb^{5+} and Sb^{5+} in the same perovskite polymorph. This is consistent with the majority of the Ba_2LnNbO_6 compounds adopting a tetragonal intermediate while the corresponding antimonates prefer the rhombohedral structure. In the series $Ba_2NdNb_{1-x}Sb_xO_6$ it appears that it is only possible to substitute up to 20 % Nb^{5+} for Sb^{5+} at the B'-site while maintaining a single phase rhombohedral structure. At the same time it is not possible to put any significant amount of Sb^{5+} into the monoclinic Ba_2NdNbO_6 structure. Outside these limits significant segregation of the Nb^{5+} and Sb^{5+} cations into two separate phases occurs. The refinements in the two phase region indicated that the amount of the two phases present is similar to the amount expected if Ba_2NdNbO_6 and Ba_2NdSbO_6 were present in the samples as two separate phases.

The nature of the phase segregation in the $Ba_2Eu_{1-x}Pr_xNb_{1-x}Sb_xO_6$ series is significantly different to that in the neodymium series. In $Ba_2NdNb_{1-x}Sb_xO_6$ the two phase region appears to be a consequence of the need for Nb^{5+} and Sb^{5+} to adopt

different structures. Given the similarities in size and charge of Nb^{5+} and Sb^{5+} (ionic radii of 0.64 and 0.60 respectively[5]) this must reflect a bonding difference. The volumes of the two end-members are very similar indicating the structure has insufficient flexibility to compensate for this. While a solubility limit also exists in the $Ba_2Eu_{1-x}Pr_xNb_{1-x}Sb_xO_6$ oxides tuning of the effective size of the B-site lanthanide cation across the series evidently gives additional structural flexibility. This results in a smaller miscibility gap but, critically, introduces a third monoclinic structure as one part of the two phase mixture. The specific mechanism by which the tuning of the lanthanide size affects the size of the miscibility gap is, at present, unclear. This suggests that phase transitions from tetragonal to monoclinic and then to rhombohedral symmetry occur across this system with partial segregation in the two phase region. For both series the segregation into two phases is more energetically favourable than forcing the Sb^{5+} and Nb^{5+} cations into an unfavoured geometry.

The solubility of Nb^{5+} in the rhombohedral phase of $Ba_2Eu_{1-x}Pr_xNb_{1-x}Sb_xO_6$ is high, up to 50 % of the B'-site cation sites with no segregation into a second phase. There are, however, no single phase members of this series that contain Sb^{5+} in a tetragonal *I*4/*m* structure. The low solubility of Sb^{5+} cations in the niobate structure in both series could be interpreted as being a result of Sb^{5+} having a full *d*-shell that does not allow it to participate in π-bonding using these orbitals. As presented in Chapter 3 π-bonding is considered to be important to stabilising the tetragonal structure as opposed to rhombohedral symmetry in the $Ba_2LnB'O_6$ series. It is expected that π-bonding would also be important in the monoclinic niobate structure. This observation provides an explanation for the chemical incompatibility of the Nb^{5+} and Sb^{5+} cations. In particular the low solubility of the Sb^{5+} cations in the niobate phases is likely a result of the interruption of the π-bonding in the niobate structure caused by the presence of significant levels of Sb^{5+} cations.

4.5 Conclusions

The phases present in $Ba_2Eu_{1-x}Pr_xNb_{1-x}Sb_xO_6$ and $Ba_2NdNb_{1-x}Sb_xO_6$ have been examined using synchrotron X-ray diffraction. It has been found that the $Ba_2Eu_{1-x}Pr_xNb_{1-x}Sb_xO_6$ series exhibits a series of phases from *I*4/*m* tetragonal to *I*2/*m*

monoclinic to $R\bar{3}$ rhombohedral with increasing x. The monoclinic structure only exists as part of a two phase mixture with one of the other structures over the range of $0.1 \leq x \leq 0.4$. Variable temperature X-ray diffraction and EDX analysis indicates that this two phase region is a result of partial segregation of Nb^{5+} and Sb^{5+} into separate phases. The $Ba_2NdNb_{1-x}Sb_xO_6$ series has been found to exhibit extensive phase segregation, consisting of two phase mixtures of the end-member monoclinic (x = 0) and rhombohedral (x = 1) structures over the range $0.1 \leq x \leq 0.7$. This larger miscibility gap is presumably due to the lack of tuning of the lanthanide size. In the case of both series the Sb^{5+} cations are found to have much lower solubility in the niobate structure than the Nb^{5+} cations have in the $R\bar{3}$ structure. This is likely to be related to the Sb^{5+} substitution disrupting the π-bonding required to stabilize the tetragonal niobate structure hence making segregation energetically favourable.

4.6 References

[1] M. Retuerto, M. García-Hernández, M.J. Martínez-Lope, M.T. Fernández-Díaz, J.P. Attfield, J.A. Alonso, J. Mater. Chem. 17 (2007) 3555-3561.

[2] J.M.D. Coey, M. Viret, S. von Molnár, Adv. Phys. 48 (1999) 167-293.

[3] B. Jaffe, R.S. Roth, S. Marzullo, J. Appl. Phys. 25 (1954) 809-810.

[4] R. Guo, L.E. Cross, S.-E. Park, B. Noheda, D.E. Cox, G. Shirane, Phys. Rev. Lett. 84 (2000) 5423-5426.

[5] R.D. Shannon, Acta Cryst. A 32 (1976) 751-767.

[6] B.J. Kennedy, C.J. Howard, K.S. Knight, Z. Zhang, Q. Zhou, Acta Cryst. B 62 (2006) 537-546.

[7] J.A. Alonso, E. Mzayek, I. Rasines, J. Solid State Chem. 84 (1990) 16-22.

[8] R. Macquart, B.J. Kennedy, T. Vogt, C.J. Howard, Phys. Rev. B: Condens. Matter 66 (2002) 212102.

[9] R.H. Mitchell, *Perovskites Modern and Ancient*, Almaz Press, Ontario, 2002.

[10] V.M. Goldschmidt, Naturwissenschaften 14 (1926) 477-485.

[11] R.H. Mitchell, A.R. Chakhmouradian, P.M. Woodward, Phys. Chem.Miner. 27 (2000) 583-589.

[12] C.J. Howard, B.J. Kennedy, P.M. Woodward, Acta Cryst. B 59 (2003) 463-471.

[13] W.T.A. Harrison, K.P. Reis, A.J. Jacobson, L.F. Schneemeyer, J.V. Waszczak, Chem. Mater. 7 (1995) 2161-2167.